

9-14-2004

Effect of wetting layers on the strain and electronic structure of InAs self-assembled quantum dots

Seungwon Lee
Jet Propulsion Laboratory

Olga L. Lazarenkova
Jet Propulsion Laboratory

Paul von Allmen
Jet Propulsion Laboratory

Fabiano Oyafuso
Jet Propulsion Laboratory

Gerhard Klimeck
Purdue University - Main Campus, gekco@purdue.edu

Follow this and additional works at: <http://docs.lib.purdue.edu/nanodocs>

Lee, Seungwon; Lazarenkova, Olga L.; von Allmen, Paul; Oyafuso, Fabiano; and Klimeck, Gerhard, "Effect of wetting layers on the strain and electronic structure of InAs self-assembled quantum dots" (2004). *Other Nanotechnology Publications*. Paper 122.
<http://docs.lib.purdue.edu/nanodocs/122>

This document has been made available through Purdue e-Pubs, a service of the Purdue University Libraries. Please contact epubs@purdue.edu for additional information.

Effect of wetting layers on the strain and electronic structure of InAs self-assembled quantum dots

Seungwon Lee,* Olga L. Lazarenkova, Paul von Allmen, Fabiano Oyafuso, and Gerhard Klimeck†
Jet Propulsion Laboratory, California Institute of Technology, Pasadena, California 91109, USA

(Received 8 April 2004; revised manuscript received 16 June 2004; published 14 September 2004)

The effect of wetting layers on the strain and electronic structure of InAs self-assembled quantum dots grown on GaAs is investigated with an atomistic valence-force-field model and an empirical tight-binding model. By comparing a dot with and without a wetting layer, we find that the inclusion of the wetting layer weakens the strain inside the dot by only 1% relative change, while it reduces the energy gap between a confined electron and hole level by as much as 10%. The small change in the strain distribution indicates that strain relaxes only little through the thin wetting layer. The large reduction of the energy gap is attributed to the increase of the confining-potential width rather than the change of the potential height. First-order perturbation calculations or, alternatively, the addition of an InAs disk below the quantum dot confirm this conclusion. The effect of the wetting layer on the wave function is qualitatively different for the weakly confined electron state and the strongly confined hole state. The electron wave function shifts from the buffer to the wetting layer, while the hole shifts from the dot to the wetting layer.

DOI: 10.1103/PhysRevB.70.125307

PACS number(s): 73.21.La

I. INTRODUCTION

Nanometer-size semiconductor quantum dots are the subject of a rapidly developing area in semiconductor research, as they provide an increase in the speed of operation and a decrease in the size of semiconductor devices.¹ One of the prominent fabrication methods for quantum dots is the Stranski-Krastanov process. This method uses the relief of the elastic energy when two materials with a large lattice mismatch form an epitaxial structure. During the epitaxial growth, the deposited material initially forms a thin epitaxial layer known as the wetting layer. As more atoms are deposited on the substrate, the elastic energy becomes too large to form a dislocation-free layer, leading to the formation of a cluster to relieve some of the elastic energy. In this manner, a quantum dot is “self-assembled” on top of the wetting layer.

Although the self-assembled dot is grown on top of the wetting layer, some theoretical studies omit the wetting layer from their simulations without much justification.^{2–10} Other studies including the wetting layer discuss little about its influence on the properties of the self-assembled dots.^{11–17} In this paper we aim at presenting a more complete discussion of the effect of wetting layers on the properties of self-assembled quantum dots. In particular, we address two issues: (i) How does the wetting layer affect the strain distribution in InAs/GaAs self-assembled dots? (ii) How does the wetting layer affect the electronic structure of the quantum dots? To answer the first question, we model the elastic energy with a valence-force-field (VFF) model developed by Keating.¹⁸ For the second question, we model the electronic structure with an $sp^3d^5s^*$ empirical tight-binding model. The tight-binding parameters depend on the inter-atomic positions in order to incorporate the strain effect. The VFF and tight-binding model enables us to describe the dot geometry, interface, and strain effect at the atomic level.

II. MODEL

A. Strain profile

Within an atomistic VFF model,¹⁸ the elastic energy depends on the length and angle of the bonds that each atom makes with its nearest neighbors. For each atom i , the elastic energy is given by

$$E_i = \sum_j \frac{3\alpha}{8r_0^2} (\vec{r}_{ij}^2 - r_0^2)^2 + \sum_{\langle jk \rangle} \frac{3\beta}{8r_0^2} \left(\vec{r}_{ij} \cdot \vec{r}_{ik} + \frac{r_0^2}{3} \right)^2. \quad (1)$$

Here, \vec{r}_{ij} is the vector connecting the atom i to one of its nearest neighbors j , r_0 is the unstrained bond length, and α and β are the atomic elastic constants for bond stretch and bond bend, respectively. The atomic constants are related to the constants (C_{11}, C_{12}, C_{44}) of the continuum elasticity theory:

$$C_{11} = \frac{\alpha + 3\beta}{a}, \quad C_{12} = \frac{\alpha - \beta}{a}, \quad C_{44} = \frac{4\alpha\beta}{a(\alpha + \beta)}, \quad (2)$$

where a is the lattice constant. All three of the continuum constants cannot be perfectly fitted with only two atomic constants α and β .¹⁹ For this work, the atomic elastic constants are taken from Ref. 20. The resulting C_{11} and C_{12} from Eq. (2) fit the measured values within a few percent error, while the resulting C_{44} differs from the experimental value by about 10% for GaAs and 20% for InAs.²¹ Constants C_{11} and C_{12} are related to hydrostatic and biaxial strain, while C_{44} is related to shear strain. For self-assembled quantum dots where hydrostatic and biaxial stress are overall stronger than shear stress, an accurate description of C_{11} and C_{12} is more important than that of C_{44} . To improve the description of C_{44} , long-range Coulomb interactions should be included in the elastic energy.¹⁹

B. Electronic structure

In the framework of an empirical tight-binding model, the effective electron Hamiltonian is described with a basis of $sp^3d^5s^*$ orbitals and two spin states per atom, including nearest-neighbor interactions between the orbitals and including the spin-orbit coupling:

$$H = \sum_{i,\gamma,s} \epsilon_{i,\gamma} |i,\gamma,s\rangle \langle i,\gamma,s| + \sum_{i,j,\gamma,\gamma',s} t_{i,\gamma,j,\gamma'} |i,\gamma,s\rangle \langle j,\gamma',s| + \sum_{i,\gamma,\gamma',s,s'} \lambda_{i\gamma s;i\gamma' s'} |i,\gamma,s\rangle \langle i,\gamma',s'|, \quad (3)$$

where i and j index atoms, γ and γ' index orbital types, and s and s' index spins. Parameters $\epsilon_{i,\gamma}$ denote the atomic energy, $t_{i,\gamma,j,\gamma'}$ the neighbor-interaction, and $\lambda_{i\gamma s;i\gamma' s'}$ the spin-orbit coupling. The tight-binding parameters $\epsilon_{i,\gamma}$, $t_{i,\gamma,j,\gamma'}$, $\lambda_{i\gamma s;i\gamma' s'}$ are first determined by fitting the band edge energies and effective masses of the unstrained bulk InAs and GaAs crystals, using a genetic optimization algorithm.^{22,23} The resulting tight-binding parameters produce the correct band edge energies to within a 0.1% accuracy and the correct effective mass to within a 10% accuracy.

In order to incorporate the effect of the altered atomic environment due to strain, the tight-binding parameters are modified. We use the model developed by Boykin *et al.* as follows.²² For the neighbor-interaction energy $t_{i,\gamma,j,\gamma'}$, the direction cosines in the Slater-Koster table are used to describe the effect of the bond bend. The magnitude of the two-center integrals in the Slater-Koster table is scaled to incorporate the effect of the bond stretch: $U = U_0(d_0/d)^\eta$, where U_0 is the unstrained-crystal two-center integral, and d_0 and d are the unstrained and strained bond lengths, respectively. For the atomic energy $\epsilon_{i,\gamma}$, the Löwdin orthogonalization procedure is used to obtain the modified atomic energy in a strained environment:

$$\epsilon_{i,\gamma} = \epsilon_{i,\gamma}^{(0)} + \sum_{j,\gamma'} K_{i,\gamma,j,\gamma'} \frac{(t_{i,\gamma,j,\gamma'}^{(0)})^2 - (t_{i,\gamma,j,\gamma'})^2}{\epsilon_{i,\gamma}^{(0)} + \epsilon_{j,\gamma'}^{(0)}}. \quad (4)$$

Here, j is the index for neighboring atoms. The superscript (0) represents the energies for the unstrained crystal. The modified atomic energy depends both on neighbor-atom energies and neighbor-interaction energy. The description of strained materials introduces two types of new parameters: a scaling exponent η for each two-center integral and an atomic energy shift constant K . The new parameters η and K are determined by fitting the band edge energies under hydrostatic and uniaxial strain.^{22,23} The resulting parameters describe the band-edge-energy dependency on hydrostatic and uniaxial strain (i.e., deformation potential) to within a 10% accuracy. Considering the uncertainty of the experimental values and a wide disagreement among the theoretical predictions for the deformation potential,²⁴ the accuracy of 10% is reasonable.

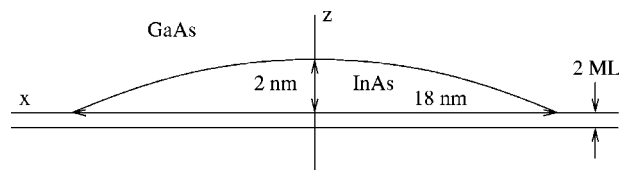


FIG. 1. Geometry of an InAs quantum dot with a wetting layer. The dot is lens shaped with a base diameter of 18 nm and a height of 2 nm. The wetting layer is 2 ML thick, which is roughly 0.6 nm. The line x and z are the lines along which the strain profiles are plotted in Fig. 2.

III. WETTING-LAYER EFFECT

A. Strain profile

We model a lens-shaped InAs quantum dot with a base diameter of 18 nm and a height of 2 nm, as shown in Fig. 1. The geometry of a quantum dot grown by molecular beam epitaxy varies widely with the growth condition.^{25–28} The dot geometry chosen for this work is within the experimentally achievable range.^{25,29} It is known that strain in InAs/GaAs heterostructures penetrates deeply into the GaAs substrate.^{13,20,30} To accommodate the long-ranged strain relaxation, we include a large GaAs buffer ($60 \times 60 \times 40$ nm box) surrounding the InAs dot. A periodic boundary condition is imposed at the boundary for the strain calculation. Minimizing the total elastic energy with respect to atomic displacements yields a strain distribution in the InAs/GaAs self-assembled quantum dots.

Figure 2 shows the resulting strain profile along the growth direction and in the growth plan (see lines x and z in Fig. 1). The strain penetrates into the GaAs buffer as deeply as 15 nm along the growth direction, and as widely as 5 nm in the growth plane. To illustrate the effect of the wetting layer on the strain distribution, the strain profiles of the dot with and without a wetting layer are plotted together in Fig. 2. Besides the wetting layer region, the two strain profiles are almost identical within about a 1% relative difference. For example, the inclusion of the wetting layer slightly changes ϵ_{zz} from 0.0333 to 0.0330, and ϵ_{xx} from -0.0653 to -0.0647 at the center of the dot. This small change shows that the strain does not relax efficiently through the thin wetting layer. Figure 2 also shows that shear strain ϵ_{xz} reaches 0.02 near the interface between InAs and GaAs in the growth plane.³¹ Although the interface geometry is different between the QD and the QD-WL structures, their shear strain distribution is almost identical. Overall, the wetting layer does not change the strain distribution in the InAs dot and the GaAs buffer in terms of both hydrostatic/biaxial strain (ϵ_{ii}) and shear strain (ϵ_{ij}).

B. Potential profile

Within the strained structure, we calculate its local potential profile. The potential profile is obtained by computing the band structure for a periodic lattice with the geometry of the local strained unit cell. Figure 3 shows the conduction and valence band edges of each unit cell along the growth direction [001]. The valence band edge of unstrained GaAs is

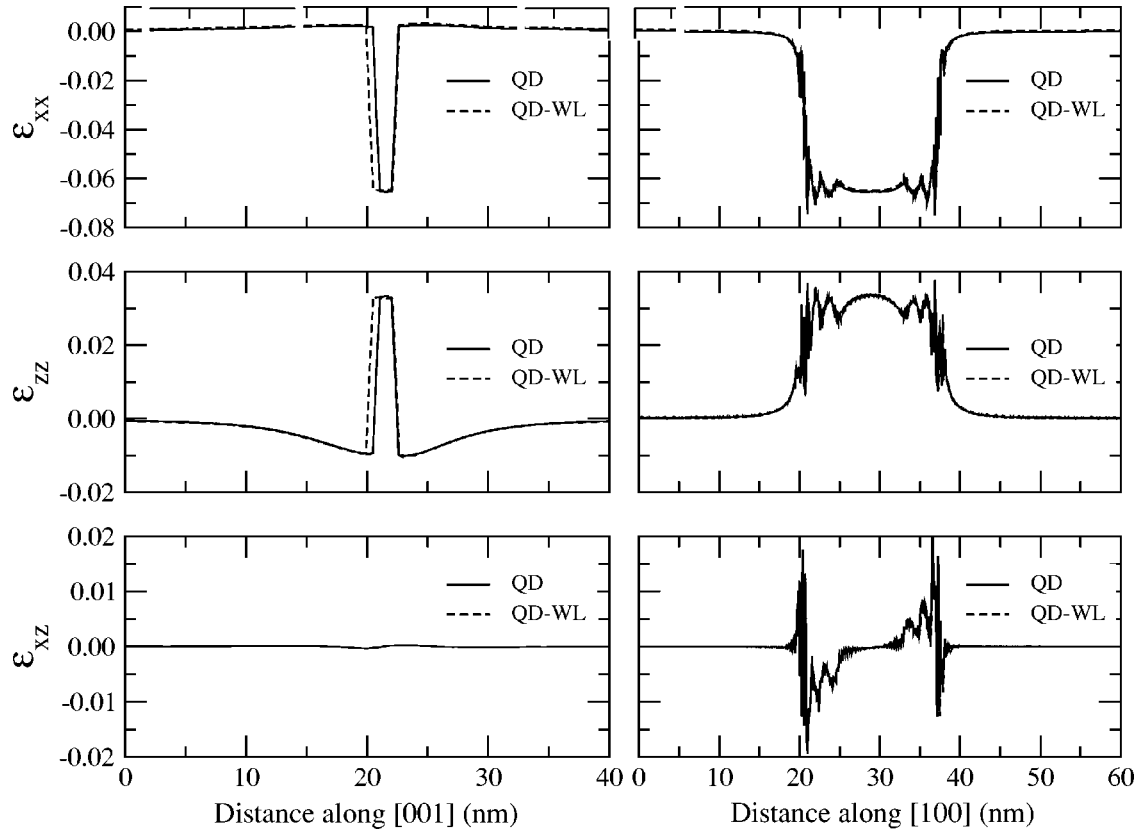


FIG. 2. Strain profiles of a quantum dot without a wetting layer (QD) and with a wetting layer (QD-WL) along [001] and [100]. The strain profiles are calculated by imposing a periodic boundary condition to a large GaAs buffer ($60 \times 60 \times 40$ nm box) surrounding the quantum dot. Besides the wetting layer region, the two strain profiles are almost identical with only a 1% relative difference. This shows that strain does not relax efficiently through the thin wetting layer, and consequently the wetting layer does not change the strain distribution in the dot and the buffer.

set to be zero as a reference energy. Strain effects are significant on both conduction and valence bands. The conduction band edge in the strained dot shifts up from 0.6 eV (unstrained InAs conduction band edge) to 1.0 eV, while the valence band edge splits to two branches, the heavy- and light-hole bands separated by 0.2 eV. The valence band edge for unstrained InAs is 0.23 eV. The order of the heavy- and light-hole bands in the dot is opposite the order in the buffer, because the biaxial components $\epsilon_{xx} + \epsilon_{yy} - 2\epsilon_{zz}$ of the dot strain and the buffer strain have an opposite sign.

The difference in the potential profiles for a quantum dot without a wetting layer (QD) and a dot with a wetting layer (QD-WL) is illustrated in Fig. 3. The inclusion of the wetting layer extends the width of the confining potential well, but hardly modifies the height of the potential well. The change in the potential height is about 1 meV. The small change is consistent with the small difference in their strain profiles. Due to the change of the material, the potentials in the wetting layer region differ by 0.44 eV for the conduction band, and by 0.36 eV for the heavy-hole band.

C. Single-particle energies

We next calculate the confined single-particle energies for the QD and QD-WL structures. The single-particle energies

are calculated with a truncated GaAs buffer ($30 \times 30 \times 15$ nm box) instead of the large GaAs buffer ($60 \times 60 \times 40$ nm box) used for the strain calculation. This method takes advantage of the spatial localization of the confined states, and significantly reduce the required computation time. An energy convergence of 1 meV is obtained by varying the truncated buffer size. To eliminate spurious surface states in the artificially truncated buffer, the dangling-bond energies of surface atoms are raised by 10 eV.³² This surface treatment efficiently eliminates all the spurious surface states without changing the confined states of interest.³²

Table I lists the calculated single particle energies relative to the GaAs valence band edge. As the wetting layer is included, the lowest electron energy shifts down by 64 meV and the highest hole energy shifts up by 46 meV, leading to the reduction of the energy gap by 110 meV (9% relative change). As a first-order effect, these shifts are attributed to an increase of the width of the confinement potential in the vertical direction [001]. To estimate the effect of the width change, we calculate the single-particle energies for a quantum dot with a disk beneath the dot (QD-Disk). The disk thickness is the same as the thickness of the wetting layer. The energies of QD-Disk are closer to those of QD-WL than to those of QD. The difference between the energies of QD-Disk and QD-WL is attributed to the wetting layer region beyond the disk region.

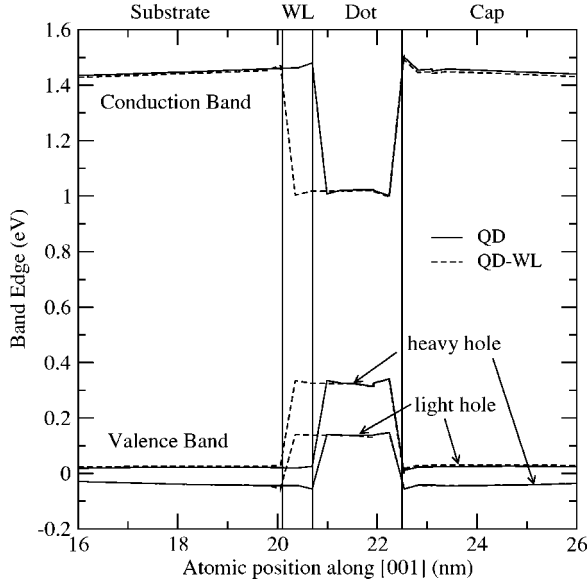


FIG. 3. Potential profiles of a quantum dot without a wetting layer (solid line) and a quantum dot with a wetting layer (dashed line). The potential profiles are obtained by calculating the conduction and valence band edges of the local strained unit cells along the growth direction [001]. Beside the wetting layer region, the band edges for the two nanostructures are almost identical within 1 meV variation. This shows that the inclusion of the wetting layer primarily extends the width of the confining potential well without modifying the height of the potential well.

As another approximation for the wetting layer effect, we calculate the first-order correction due to the potential change in the wetting layer region (QD-WL-Approx) as follows:

$$E_e(\text{Approx}) = E_e(\text{QD}) - 0.44 \langle \psi_e | \hat{W}L | \psi_e \rangle, \quad (5)$$

$$E_h(\text{Approx}) = E_e(\text{QD}) + 0.36 \langle \psi_h | \hat{W}L | \psi_h \rangle. \quad (6)$$

Here, $\hat{W}L$ is the operator that projects the wave function onto the wetting layer region, and ψ_e and ψ_h are the electron

TABLE I. Energies of the lowest electron (E_e) and the highest hole (E_h) levels, the corresponding energy gaps (E_{gap}), and energy spacings between the first and second lowest electron level (ΔE_e) and hole level (ΔE_h) for an InAs quantum dot without a wetting layer (QD), an InAs quantum dot with a wetting layer (QD-WL), an InAs quantum dot with an InAs disk beneath the dot (QD-Disk), and an InAs quantum dot with a first-order correction due to the potential change in the wetting layer region (QD-WL-Approx). The reference energy is the valence band edge of bulk GaAs. The energy is in the unit of eV. The geometry of the quantum dot is illustrated in Fig. 1.

Structure	E_e	E_h	E_{gap}	ΔE_e	ΔE_h
QD	1.378	0.158	1.220	0.042	0.025
QD-WL	1.314	0.204	1.110	0.042	0.022
QD-Disk	1.337	0.192	1.145	0.047	0.024
QD-WL-Approx	1.334	0.180	1.154	0.043	0.022

and hole wave functions obtained with the QD structure. Factors 0.44 eV and 0.36 eV are the shift of the effective electron and hole potential energy in the wetting layer region, respectively. The resulting energies differ from the QD-WL energies by about 20 meV. The relatively large energy difference between QD-WL-Approx and QD-WL suggests that the wave function of QD is considerably different from that of QD-WL.

In addition to the energy gap, the effect of the wetting layer on excited electron and hole levels is analyzed. As for the electron, the quantum dot without a wetting layer accommodates three bound levels, which are one s -like level and two p -like levels (excluding the spin degeneracy). The inclusion of the wetting layer results in two additional bound levels with d -like symmetry. The two p -like levels are aligned along $[110]$ and $[1\bar{1}0]$ directions, and are slightly split by 0.4 meV, resulting from the anisotropy of the potential along $[110]$ and $[1\bar{1}0]$ directions. We speculate that the anisotropy originates from the asymmetry of the potential near the interface and is propagated from the interface to the dot center through the strain relaxation. The two d -like levels have the symmetry of d_{xy} and $d_{x^2-y^2}$, and are split by 4 meV due to the zinc-blende crystal field. The hole has more bound levels than the electron due to its larger effective mass, but the symmetry and degeneracy of the first few hole levels are similar to those of the electron levels.

The energy spacings between the ground level (s -like) and the first excited level (p -like) with and without the wetting layer are compared for the electron and hole. As listed in Table I, the electron energy spacing ΔE_e remains the same, while the hole energy spacing ΔE_h changes by 3 meV (12% relative change). The energy spacings are determined mainly by the lateral confinement rather than the vertical confinement, because lens-shaped self-assembled quantum dots have a large aspect ratio. No change in ΔE_e suggests that the wetting layer does not change the effective lateral confinement range for the electron. In contrast, the decrease of ΔE_h suggests that the wetting layer increases the lateral confinement range for the hole.

We further study the energy gap and spacing change with respect to the ratio γ_h of the dot height to the wetting-layer height. For a quantum dot with a larger height (4 nm) and the same base diameter (18 nm), the inclusion of the wetting layer (still 2 ML thick) leads to the change of the gap from 1.103 eV to 1.050 eV (5% change), ΔE_e from 0.051 eV to 0.047 eV (8% change), and ΔE_h from 0.023 eV to 0.019 eV (17% change). In comparison to the small dot discussed above (see Table I), the change in the gap is smaller for the large dot, while the change in the spacing is larger. This illustrates that the effect of the wetting layer on the energy gap and spacing is sensitive to the height ratio γ_h . The smaller change in the gap can be explained by the small relative change in the confinement potential width in the vertical direction. The larger change in the spacing is related to the fact that the electron and hole are more efficiently localized in the large dot than in the small dot. When the wetting layer is included, the localized wave functions spread to the wetting layer, leading to a larger spatial extent in the lateral direction and thus to a small energy spacing.

TABLE II. Distribution of the lowest electron and the highest hole wave functions for a quantum dot without a wetting layer (QD) and a quantum dot with a wetting layer (QD-WL). The weights of the wave function in the InAs dot, the InAs wetting layer, and the GaAs buffer region are listed. Note that the weight in the wetting layer for QD is the weight in the region where a wetting layer would be located.

Structure	Electron			Hole		
	Dot	WL	Buffer	Dot	WL	Buffer
QD	0.43	0.10	0.47	0.82	0.06	0.12
QD-WL	0.43	0.15	0.42	0.72	0.17	0.11

D. Single-particle wave functions

Since the wetting layer provides extra space for the electron and hole to be confined, the electron and hole wave functions are expected to change. The change in the wave functions is analyzed in two ways. First, the wave functions are integrated in three regions: the dot, the wetting layer, and the buffer. Table II lists the resulting weights in the three regions. The electron wave function is weakly confined in the dot region, whereas the hole wave function is strongly confined in the dot. The difference between the electron and hole wave function distributions is related to the light electron mass and the heavy hole mass. When the wetting layer is included, the electron wave function shifts from the buffer to the wetting layer. In contrast, the hole wave function shifts from the dot to the wetting layer. We find that for the large dot discussed above (height 4 nm), the electron wave function becomes more confined in the dot region and hence the effect of the wetting layer on the electron wave function distribution becomes similar to that on the hole wave function. This shows that the shift trend of the wave function due to the wetting layer is related to the degree of the localization of the wave function.

Second, the spatial extents of the wave functions are evaluated with $\sqrt{\langle |\mathbf{r} - \mathbf{r}_0|^2 \rangle}$, $\sqrt{\langle (x - \langle x \rangle)^2 \rangle}$, and $\sqrt{\langle (z - \langle z \rangle)^2 \rangle}$, where \mathbf{r}_0 is the center of mass given by $(\langle x \rangle, \langle y \rangle, \langle z \rangle)$. The calculated expectation values are listed in Table III. The spatial extent of the electron function is relatively unchanged, while the extent of the hole wave function increases by 0.46 nm. These trends are consistent with the wave function weight shifts listed in Table II. The hole wave function spreads from the dot to the wetting layer, leading to a larger spatial extent in both lateral and vertical dimensions. In contrast, the electron wave function moves from the buffer to the wetting layer, leading to a smaller spatial extent in the vertical dimension and a larger spatial extent in the lateral dimension.

We also observe from the center of mass $\langle z \rangle$ that both the electron and hole wave function move toward the bottom of the dot by 0.3 nm, when the wetting layer is included. However, the relative distance between the electron's and the hole's center of mass is unchanged. For both QD and QD + WL, the hole's center of mass is above the electron's by 0.04 nm, which was observed by a Stark effect experiment.³³

TABLE III. Spatial extents of the lowest electron and the highest hole wave functions for a quantum dot without a wetting layer (QD) and a quantum dot with a wetting layer (QD-WL). The QD base diameter is 18 nm, the QD height 2 nm, and the WL thickness 2 ML. The spatial extents are estimated with $\Delta r = \sqrt{\langle |\mathbf{r} - \mathbf{r}_0|^2 \rangle}$, $\Delta x = \sqrt{\langle (x - \langle x \rangle)^2 \rangle}$, and $\Delta z = \sqrt{\langle (z - \langle z \rangle)^2 \rangle}$, where \mathbf{r}_0 is the position vector of the center of mass, that is given by $(\langle x \rangle, \langle y \rangle, \langle z \rangle)$. The listed $\langle z \rangle$ is the distance of the center of mass from the dot base, and $\langle x \rangle$ and $\langle y \rangle$ coincide with the dot center. The listed values are in units of nm.

Structure	State	Δr	Δx	Δz	$\langle z \rangle$
QD	Electron	4.99	3.29	1.75	0.71
QDWL	Electron	4.97	3.36	1.54	0.41
QD	Hole	3.43	2.37	0.70	0.75
QDWL	Hole	3.89	2.70	0.73	0.45

An empirical pseudopotential calculation shows that the electron-hole alignment depends on the size, shape, and In/Ga composition profile.^{3,16} An eight-band $\mathbf{k} \cdot \mathbf{p}$ calculation predicts the measured alignment, hole above electron, only when gallium diffusion is introduced near the top of the dot.⁷

IV. DISCUSSION

In this section, we discuss the effect of the wetting layer on other properties of quantum dots besides strain, single-particle energy, and single-particle wave function. Since the wetting layer considerably affects the single-particle wave function, the wetting layer is also expected to influence the electrical and optical properties of self-assembled quantum dots. For example, the overlap between the electron and hole wave function in the wetting layer increases fourfold when the wetting layer is included (see Table II). This will affect the oscillator strengths and photoluminescence polarization for inter-band transitions. Furthermore, the spatial extent of the hole wave function increases, while that of the electron wave function remains the same (see Table III). This will lead to a weaker excitonic binding energy. Finally, the spatial extents of the wave functions in the vertical direction determines the coupling between stacked quantum dots. When the wetting layer is included, the vertical extent of the hole wave function increases, while that of the electron wave function decreases (see Table III). This will lead to a larger inter-dot coupling for hole levels but a smaller inter-dot coupling for electron levels.

In the present study we do not take into account a non-uniform In/Ga composition profile in the self-assembled dot. A large amount of In/Ga intermixing near the interface, induced by a high growth temperature and post-growth thermal annealing, has been observed in self-assembled quantum dots. The main consequence of the In/Ga intermixing for this investigation is that the confinement potential becomes a gradually varying function rather than an abruptly-changing function near the interface as shown in Fig. 3. Although the lower In content in the dot and the wetting layer blue-shifts the energy gap, we do not expect that the inclusion of the In/Ga intermixing alters the qualitative conclusion about the

TABLE IV. Excitonic energy shell structure of self-assembled InGaAs quantum dots. The present calculation with the tight-binding (TB) model is compared with a pseudopotential (PP) calculation and a photoluminescence (PL) measurement. To compare with the energy of PL peaks, the energy spacing between the electron and hole level with the same symmetry is listed for the calculation. Symbols e and h stand for the electron and hole level, respectively. Subscripts s , p , and d represent the symmetry of the wave function. The dot geometries of the PP calculation and the experiment are slightly different from the present dot geometry. The listed exciton energies for the experiment include an electron-hole binding energy, while the listed energies for the present and pseudopotential calculations do not. The pseudopotential calculations predict that the electron-hole binding energy for the lowest exciton level is 35 meV.

Geometry In/Ga composition	TB calc. 18×2 nm InAs	PP calc. ^a 25×2.5 nm InAs	Exp. ^b 20×3 nm InGaAs ^c
e_s-h_s	1.110	1.166	1.25
e_p-h_p	1.175	1.251	1.30
e_d-h_d	1.231	1.332	1.35

^aFrom Ref. 3

^bFrom Ref. 34

^cAn exact composition ratio of the dot is not known, but a significant amount of In/Ga intermixing is expected due to its high annealing temperature 850 °C.

effect of the wetting layer on the strain and the electronic structure of the self-assembled quantum dot.

We finish the discussion by comparing the present results with relevant results from other theoretical calculations and experiments. No theoretical or experimental work studies exactly the same quantum dot as our modeled dot in terms of geometry and composition profile. Hence, the comparison is applied to results available for a similar quantum dot: a pseudopotential calculation for a lens-shaped dot with base diameter 25 nm and height 2.5 nm without wetting layer³ and a recent photoluminescence measurement for highly homogeneous quantum dots with base diameter 20 nm and height 3 nm and obviously with wetting layer.³⁴ Table IV shows that the present tight-binding model generally underestimates the exciton energy. This disagreement can be attributed to the absence of In/Ga intermixing in our model.

On the other hand, the spacing between the exciton levels agrees better with the experiment.

V. CONCLUSION

In summary, the effect of wetting layers on the strain and electronic structure of InAs self-assembled quantum dots is investigated with an atomistic valence-force-field model and an $sp^3d^5s^*$ empirical tight-binding model. By comparing a dot with and without a wetting layer, we find that the inclusion of the wetting layer weakens the strain inside the dot by only a 1% relative change while it reduces the energy gap between the confined electron and hole states by as much as 10%.

The small change in the dot strain indicates that strain relaxes little through the thin wetting layer. Overall, the wetting layer does not change the strain distribution in the self-assembled quantum dot. The large reduction of the energy gap in the quantum dot with a wetting layer is attributed to the increase in the width of the confining potential rather than the change in the height of the potential. First order perturbation calculations or, alternatively, the addition of an InAs disk below the quantum dot confirm this conclusion. In a thin quantum dot, the effect of the wetting layer on the wave function is qualitatively different for the weakly confined electron and the strongly confined hole states. The electron wave function moves from the buffer to the wetting layer, while the hole wave function spreads from the dot to the wetting layer region. The redistribution of the hole wave function causes the increase of the effective lateral confinement range and thus the decrease of the hole level spacing ΔE_h . Since the wetting layer considerably affects both the single-particle energy and wave function, the wetting layer should be included in the model in order to accurately model the electric and optical properties of a single self-assembled dot and coupled quantum dots.

ACKNOWLEDGMENTS

This work was performed at the Jet Propulsion Laboratory, California Institute of Technology under a contract with the National Aeronautics and Space Administration. Funding was provided under grants from ARDA, JPL Bio-Nano program, and the NSF (Grant No. EEC-0228390). One of the authors (O. L. L.) held a National Research Council Research Associateship Award at JPL.

*Electronic address: Seungwon.Lee@jpl.nasa.gov

[†]Also at the Network for Computational Nanotechnology, School of Electrical and Computer Engineering, Purdue University, West Lafayette, Indiana 47906, USA.

¹D. Bimberg, M. Grundmann, and N. Ledentsov, in, *Quantum Dot Heterostructures* (Wiley, New York, 1998).

²M. Califano and P. Harrison, Phys. Rev. B **61**, 10 959 (2000).

³A. J. Williamson, L.-W. Wang, and A. Zunger, Phys. Rev. B **62**, 12 963 (2000).

⁴A. J. Williamson and A. Zunger, Phys. Rev. B **59**, 15 819 (1999).

⁵C. Pryor, Phys. Rev. B **57**, 7190 (1998).

⁶C. Pryor, Phys. Rev. B **60**, 2869 (1999).

⁷W. Sheng and J.-P. Leburton, Phys. Rev. B **63**, 161301 (2001).

⁸W. Sheng and J.-P. Leburton, Phys. Rev. B **64**, 153302 (2001).

⁹W. Sheng and J.-P. Leburton, Phys. Rev. B **67**, 125308 (2003).

¹⁰C. E. Pryor and M. E. Flatte, Phys. Rev. Lett. **91**, 257901 (2003).

¹¹M. Grundmann, O. Stier, and D. Bimberg, Phys. Rev. B **52**, 11 969 (1995).

- ¹²L.-W. Wang, J. Kim, and A. Zunger, Phys. Rev. B **59**, 5678 (1999).
- ¹³J. Groenen, C. Priester, and R. Carles, Phys. Rev. B **60**, 16 013 (1999).
- ¹⁴L. R. C. Fonseca, J. L. Jimenez, J. P. Leburton, and R. M. Martin, Phys. Rev. B **57**, 4017 (1998).
- ¹⁵O. Stier, M. Gruendmann, and D. Bimberg, Phys. Rev. B **59**, 5688 (1999).
- ¹⁶J. Shumway, A. Williamson, A. Zunger, A. Passaseo, M. DeGiorgi, R. Cingolani, M. Catalano, and P. Crozier, Phys. Rev. B **64**, 125302 (2001).
- ¹⁷R. Santoprete, B. Koiller, R. B. Capaz, P. Kratzer, Q. K. K. Liu, and M. Scheffler, Phys. Rev. B **68**, 235311 (2003).
- ¹⁸P. Keating, Phys. Rev. **145**, 637 (1966).
- ¹⁹R. M. Martin, Phys. Rev. B **1**, 4005 (1970).
- ²⁰C. Pryor, J. Kim, L. W. Wang, A. J. Williamson, and A. Zunger, J. Appl. Phys. **83**, 2548 (1998).
- ²¹O. Madelung, in *Semiconductors-Basic Data* 2nd ed. (Springer-Verlag, New York, 1996).
- ²²T. B. Boykin, G. Klimeck, R. C. Bowen, and F. Oyafuso, Phys. Rev. B **66**, 125207 (2002).
- ²³G. Klimeck, F. Oyafuso, T. B. Boyking, R. C. Bowen, and P. von Allmen, Comput. Modeling Eng. Sci. **3**, 601 (2002).
- ²⁴I. Vurgaftman, J. R. Meyer, and L. R. Ram-Mohan, Appl. Phys. Rev. **89**, 5815 (2001).
- ²⁵J. M. Moison, F. Houzay, F. Barthe, L. Leprince, E. André, and O. Vatel, Appl. Phys. Lett. **64**, 196 (1994).
- ²⁶N. P. Kobayashi, T. R. Ramachandran, P. Chen, and A. Madhukar, Appl. Phys. Lett. **68**, 3299 (1996).
- ²⁷I. Mukahametzhanov, J. Wei, R. Heitz, and A. Madhukar, Appl. Phys. Lett. **75**, 85 (1999).
- ²⁸G. S. Solomon, J. A. Trezza, A. F. Marshall, and J. J. S. Harris, Phys. Rev. Lett. **76**, 952 (1996).
- ²⁹L. Artus, R. Cusco, S. Hernandez, A. Patane, A. Polimeni, M. Henini, and L. Eaves, Appl. Phys. Lett. **77**, 3556 (2000).
- ³⁰F. Oyafuso, G. Klimeck, P. von Allmen, and T. B. Boykin, Phys. Status Solidi B **239**, 71 (2003).
- ³¹The 2% shear strain raises a question about the validity of our VFF model which has a 10–20% deviation of C_{44} from the experimental value. However, the shear strain is localized near the interface and the biaxial strain is overall dominant in the self-assembled dot.
- ³²S. Lee, P. von Allmen, F. Oyafuso, and G. Klimeck, Phys. Rev. B **69**, 045316 (2004).
- ³³P. W. Fry, I. E. Itskevich, D. J. Mowbray, M. S. Skolnick, J. J. Finley, J. A. Barker, E. P. O'Reilly, L. R. Wilson, I. A. Larkin, P. A. Maksym, M. Hopkinson, M. Al-Khafaji, J. P. R. David, A. G. Cullis, G. Hill, and J. C. Clark, Phys. Rev. Lett. **84**, 733 (2000).
- ³⁴S. Raymond, S. Studenikin, A. Sachrajda, Z. Wasilewski, S. J. Cheng, W. Sheng, P. Hawrylak, A. Babinski, M. Potemski, G. Ortner, and M. Bayer, Phys. Rev. Lett. **92**, 187402 (2004).